

1 Supporting Information

2 **Phosphorus Dopants Triggered Single-atom Platinum Catalysis**
3 **for Efficient Hydrogen Evolution in Proton Exchange Membrane**
4 **Electrolyzers**

5 Jin Peng^{a#}, Zhen Wang^{a#}, Kang Jiang^a, Ming Peng^a, Nithyadharseni Palaniyandy^b, Jianwei Ren^c, Yongwen
6 Tan^{a*}

7 ^aCollege of Materials Science and Engineering, Hunan University, Changsha, Hunan 410082, China

8 ^bInstitute for Catalysis and Energy Solutions (ICES), College of Science, Engineering, and Technology
9 (CSET), University of South Africa, Florida Science Campus, Roodepoort, 1709, South Africa

10 ^cDepartment of Chemical Engineering, Faculty of Engineering, Built Environment and Information
11 Technology, University of Pretoria , Hatfield 0028 , Pretoria, South Africa

12 [#]These authors contributed equally to this work

13 ^{*}Corresponding author

14 E-mail: tanyw@hnu.edu.cn (Y. Tan)

15

16

17

18

19

20

21

22

1 Experimental section

2 Synthesis of Catalysts

3 Synthesis of NPG:

4 NPG was obtained through etching away the Ag from Au₃₅Ag₆₅ nanosheet by etching it for 8h in 30
5 mL of 65-68% mass fraction HNO₃.^{1,2}

6 Synthesis of np-MoS₂:

7 The MoS₂@NPG composite structure was synthesized by CVD in a three-zone tubular furnace.
8 Subsequently, the MoS₂@NPG composite structure was etched to remove NPG by KI-I₂ solution (24 mg
9 I₂ and 12 mg KI dissolved in 100 mL deionized water) for 24 h to obtain np-MoS₂.

10 Synthesis of P/np-MoS₂:

11 Subsequently, P/np-MoS₂ was synthesized by further CVD in a two-zone tubular furnace. 1.0 g of
12 NaH₂PO₂·H₂O was placed in the upstream position, and the obtained MoS₂@NPG composite structure was
13 placed in the downstream position, and the temperature zone where NaH₂PO₂·H₂O located was
14 subsequently heated to 300 °C at a rate of 3 °C min⁻¹ and held for 2 h under the conditions of 90 sccm of
15 Ar and 10 sccm of H₂, meanwhile the temperature zone where the MoS₂@NPG composite structure located
16 was heated to 500 °C at a rate of 5 °C min⁻¹ and held for 2 h. P/MoS₂@NPG composite structure was
17 obtained by natural cooling, followed by etching away the NPG to obtain P/np-MoS₂.

18 Synthesis of Pt_{SA}, P/np-MoS₂:

19 Initially, 2 mg of H₂PtCl₆·6H₂O was dissolved in 50 mL of deionized water and stirred for 1 h to
20 ensure uniform dispersion of H₂PtCl₆, followed by immersion of the obtained P/np-MoS₂ sheet into it at
21 room temperature for 12 h. The obtained sheet was then transferred to carbon cloth and dried naturally at
22 room temperature and atmospheric pressure for 10 h. Finally, the sheet was placed in a vacuum drying oven
23 at 60 °C for 12 h to obtain the Pt_{SA}, P/np-MoS₂.

24 Synthesis of Pt_{SA}/np-MoS₂:

1 A similar method was employed to transfer the np-MoS₂ sheet to the same concentration of H₂PtCl₆
2 solution and then dried in the same process mentioned above to obtain a comparison sample of Pt_{SA}/np-
3 MoS₂.

4 **Structural characterizations**

5 The microscopic morphology of the prepared catalysts was identified by SEM (JEOL, JSM-
6 7610FPlus) with a volt of 10 kV. HAADF-STEM and EELS of the as-obtained catalysts were characterized
7 by TEM (Thermo Scientific, Themis Z) equipped with a focused ion beam (Thermo Scientific, Helios 5
8 CX). The chemical structure and phase characteristics of all the samples are analyzed by Raman
9 spectroscopy (Witec Alpha300R) with an excitation wavelength of 488 nm. The chemical state and
10 electronic structure of the catalysts were carried out by XPS (Thermo Scientific ESCALAB250Xi
11 spectrometer with the monochromatic Al K α). ICP-OES was performed on an Agilent 730 to obtain the
12 content of elements in the sample. The Pt L₃-edge and Mo K-edge XAS spectra were probed at the beamline
13 BL01C1 of National Synchrotron Radiation Research Center (NSRRC, NSRRC, Taiwan light source). The
14 S K-edge XAS spectra were measured at the beamline BL16A1 of NSRRC.

15 **Electrochemical measurements**

16 The HER performance of all the catalysts was evaluated by a three-electrode electrochemical system
17 utilizing a CHI-760E electrochemical workstation in 0.5 M H₂SO₄ (Sinopharm Chemical ReagentCo., Ltd,
18 95.0 %-98.0 %) at room temperature, in which the standard Ag/AgCl (saturated KCl solution) electrode as
19 the reference electrode^{3, 4}, a graphite rod as the counter electrode and the nanoporous catalysts including
20 np-MoS₂, P/np-MoS₂, Pt_{SA}/np-MoS₂, and Pt_{SA}, P/np-MoS₂ with loading of 0.5 mg cm⁻² coated on the carbon
21 cloth (1×1 cm²) as the working electrode. During the experiment, all the potentials were calibrated with a
22 Reversible Hydrogen Electrode (RHE) according to the Nernst equation ($E_{\text{RHE}} = E_{\text{Ag/AgCl}} + 0.0591 \times \text{pH} +$
23 0.197 V) and rectified manually via 95% iR compensation after the data collection ($E_{\text{iR-corrected}} = E_{\text{original}} -$
24 $95\% \times iR_s$, in which i and R_s are the current density and solution resistance, respectively). Polarization
25 curves were measured by LSV with a scan rate of 5 mV s⁻¹, and the overpotentials of HER were evaluated

1 at a current density of 10 mA cm⁻². Tafel curves were obtained based on the equation ($\eta = b \times \log j + a$, in
2 which b and j are the Tafel slope and current density, respectively). In addition, LSV and Tafel curve
3 extraction were also performed on Pt_{SA}, P/np-MoS₂ at the scan rate of 1 mV s⁻¹ to explore the effect of
4 steady-state responses on the Tafel slope.⁵ EIS was conducted with an amplitude of 10 mV from 10⁶ to 10⁻¹
5 Hz frequency range at the overpotential of 30 mV vs. RHE. The ECSA of catalysts was assessed by the C_{dl}
6 acquired from the relevant CV curves in the non-Faradaic potential region of 0.3 to 0.4 V with scan rates

7 from 10 to 100 mV s⁻¹. ECSA was computed according to the equation ($ECSA = \frac{C_{dl}}{C_s}$, C_s is the specific
8 capacitance), where the value of C_{dl} is half the slope of the line derived from linear fitting. It was found that
9 the C_s value on a flat surface is normally in the range of 20 to 60 μF cm⁻². In this paper, the C_s value was
10 uniformly assumed as 60 μF cm⁻² based on reported values.⁶ The mass activity, namely current density

11 normalized to the mass of Pt, was calculated based on the equation ($j_{mass} = \frac{j}{m_{Pt}}$). The stability of the
12 catalyst was tested by chronopotentiometry with an applied potential of 24 mV and 1000 CV cycles. The

13 Faradaic efficiency (FE) was calculated according to the equation ($FE = \frac{n_e}{n_t}$), where n_e is the amount of
14 experimentally determined H₂, n_t is the theoretically expected H₂ from the reaction. n_t was calculated by

15 applying Faraday Law ($n_t = \frac{JAt}{2F}$), where J is current density, A is the electrode area, t is time in seconds, 2

16 is number of the electrons, and F is the Faraday constant (96485.4 C/mol).⁷ FE is conducted under
17 galvanostatic electrolysis at a current density of -10 mA cm⁻². H₂ generated from the reaction was collected
18 by the water drainage method. The volume of H₂ produced was measured at different time intervals up to
19 60 min.

20 The PEMWE was constructed by assembling a self-made battery consisting of two polymethyl
21 methacrylate panels. The obtained sheet catalyst supported on Ti cloth (2 × 2 cm²) acted as the cathode.
22 The commercial IrO₂ (20 wt%) sprayed on carbon cloth (2 × 2 cm²) acted as the anode. The anode and

1 cathode were adhered together with the Nafion 117 membrane by heat pressing with a pressure of 2 MPa
 2 at 80 °C for 8 h as the membrane electrode in the PEMWE. All electrochemical tests were performed in 0.5
 3 M H₂SO₄ electrolyte.

4 The ECSA of np-MoS₂, P/np-MoS₂, Pt_{SA}/np-MoS₂, and Pt_{SA}, P/np-MoS₂ were calculated as follow:

$$5 \quad A_{ECSA}^{np-MoS_2} = \frac{47 \text{ mF cm}^{-2}}{2 \times 60 \mu\text{F cm}^{-2} \text{ per cm}_{ECSA}^2} = 391.67 \text{ cm}_{ECSA}^2$$

$$6 \quad A_{ECSA}^{P/np-MoS_2} = \frac{71 \text{ mF cm}^{-2}}{2 \times 60 \mu\text{F cm}^{-2} \text{ per cm}_{ECSA}^2} = 591.67 \text{ cm}_{ECSA}^2$$

$$7 \quad A_{ECSA}^{Pt/np-MoS_2} = \frac{130 \text{ mF cm}^{-2}}{2 \times 60 \mu\text{F cm}^{-2} \text{ per cm}_{ECSA}^2} = 1083.33 \text{ cm}_{ECSA}^2$$

$$8 \quad A_{ECSA}^{Pt,P/np-MoS_2} = \frac{141 \text{ mF cm}^{-2}}{2 \times 60 \mu\text{F cm}^{-2} \text{ per cm}_{ECSA}^2} = 1175.00 \text{ cm}_{ECSA}^2$$

9 The mass activity of Pt_{SA}/np-MoS₂, Pt_{SA}, P/np-MoS₂ and commercial Pt/C (20 wt%) were calculated
 10 as follow:

$$11 \quad j_{mass}^{Pt_{SA}/np-MoS_2} = \frac{2.50 \text{ mA cm}^{-2}}{10.24 \text{ ug cm}^{-2}} = 0.24 \text{ A mg}^{-1}$$

$$12 \quad j_{mass}^{Pt_{SA},P/np-MoS_2} = \frac{61.17 \text{ mA cm}^{-2}}{10.24 \text{ ug cm}^{-2}} = 5.97 \text{ A mg}^{-1}$$

$$13 \quad j_{mass}^{Pt/C} = \frac{29.15 \text{ mA cm}^{-2}}{50.63 \text{ ug cm}^{-2}} = 0.58 \text{ A mg}^{-1}$$

14 DFT calculations

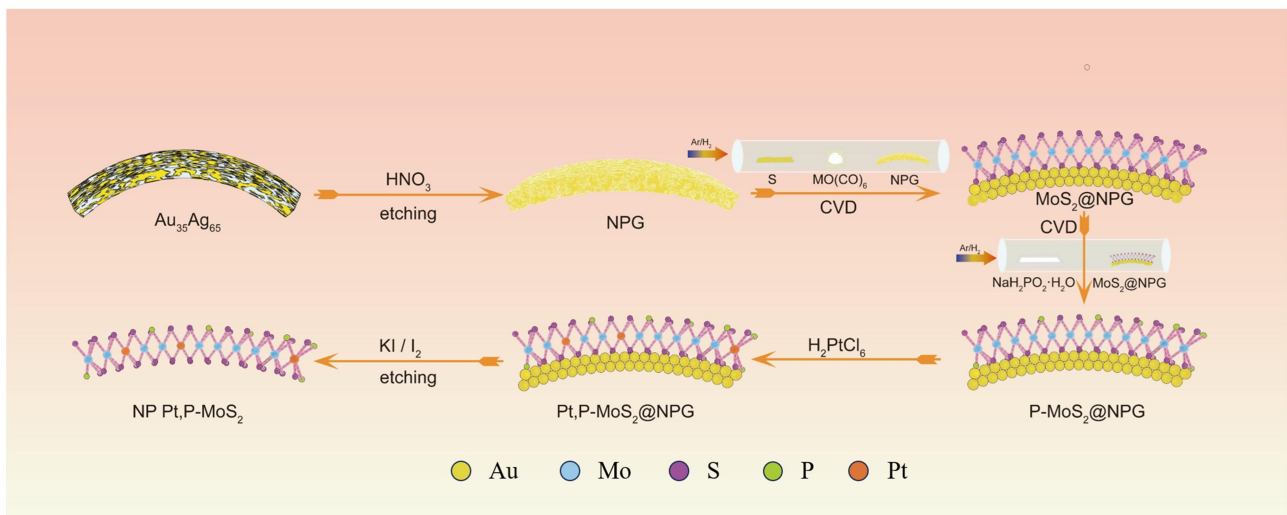
15 All computations were conducted employing DFT methods using the Vienna Ab initio Simulation
 16 Package (VASP 5.4.4)^{8, 9}. The generalized gradient approximation of Perdew-Burke-Ernzerhof (GGA-
 17 PBE) was used to describe the exchange-correlation function. The basis set utilized the projector-
 18 augmented-wave pseudopotential (PAW) method, and the plane-wave energy cutoff was set at 500 eV¹⁰,
 19 ¹¹. The MoS₂ of 2H or 1T were modeled by single-layer slabs with a (4×4) supercell, and the Monkhorst-
 20 Pack k-point sampling in the Brillouin zone was set to a (3 × 3 × 1) for calculations. Convergence was

1 assumed when forces on each atom were less than 0.02 eV/Å and the self-consistent field (SCF) tolerance
 2 was 10⁻⁶ eV in the geometry optimization. To avoid the interactions between periodic structures, the
 3 vacuum space was set to 20 Å. The DFT-D3 method with Grimme's scheme was employed to correct the
 4 van der Waals interactions¹². The Gibbs free energy of hydrogen adsorption ($\Delta G_{ad}(*H)$) was calculated
 5 by

$$G_{ad}(*H) = E(\text{Slab} + H) - E(\text{Slab}) - \frac{1}{2} * E(H_2) + \Delta ZPE - T\Delta S + \Delta H$$

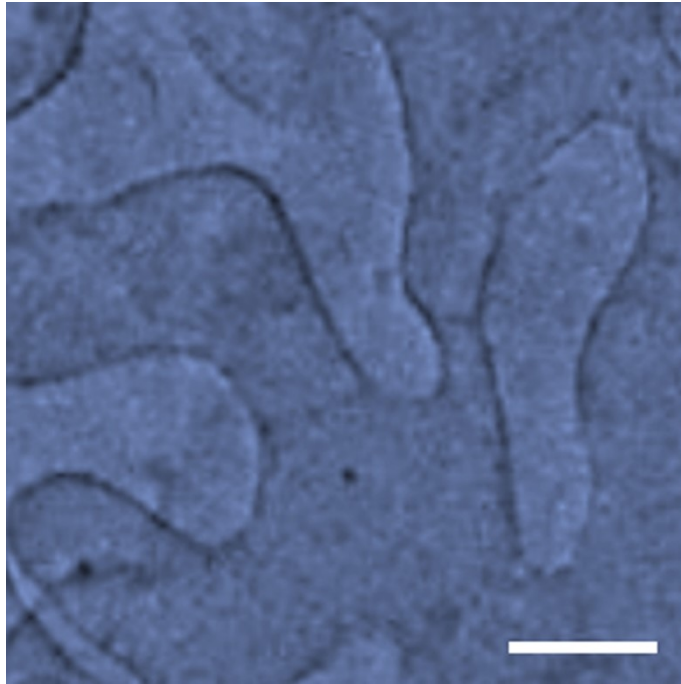
6 where $\Delta ZPE - T\Delta S + \Delta H$ for HER is about 0.24 eV¹³.

8
9
10



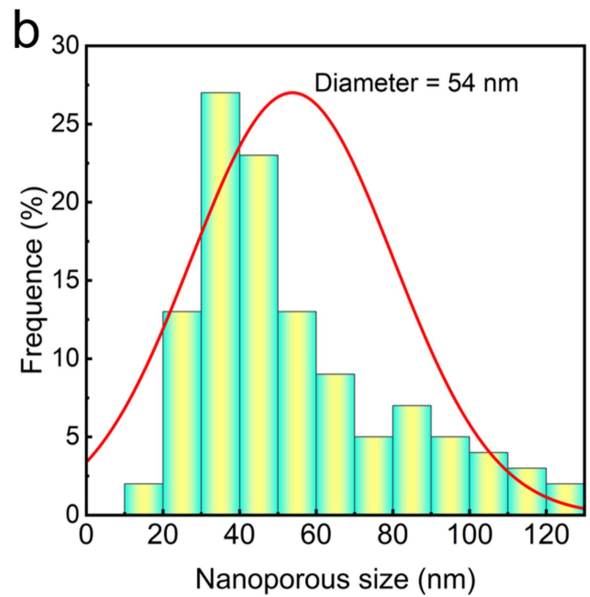
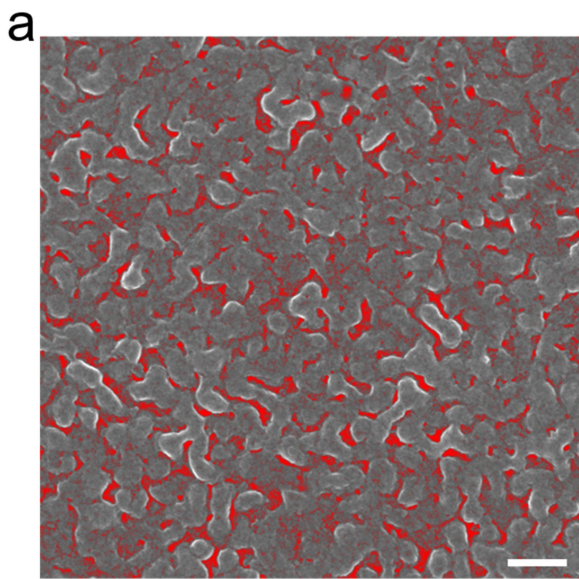
11
12 **Figure S1.** Schematic illustration of synthesis process for Pt_{SA}, P/np-MoS₂.

13
14
15



1

2 **Figure S2.** A typical TEM image of the as-prepared Pt_{SA}, P/np-MoS₂, showing the nanotube-shaped
 3 Ligaments. Scale bar: 200 nm.



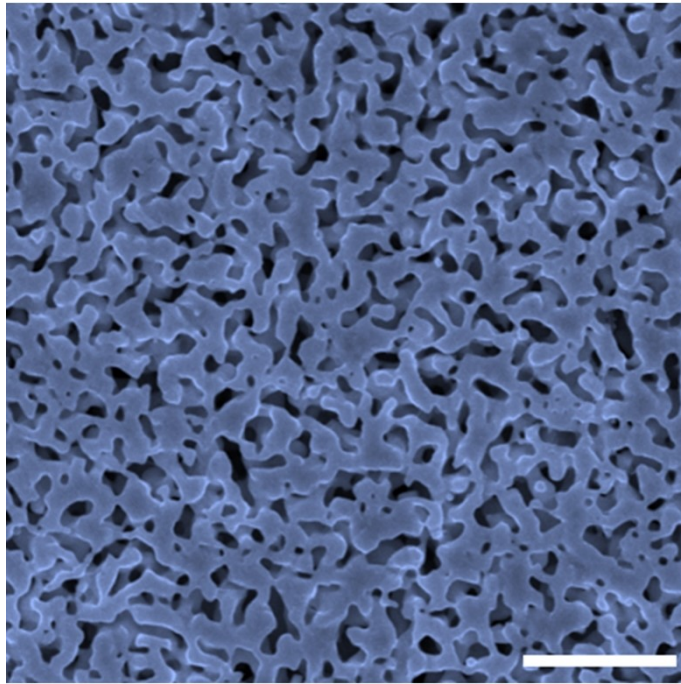
4

5 **Figure S3.** (a) A typical SEM image of the as-prepared Pt_{SA}, P/np-MoS₂. (b) The average pore diameter is
 6 measured to be 54 nm from (a). Scale bar: 100 nm.

7

8

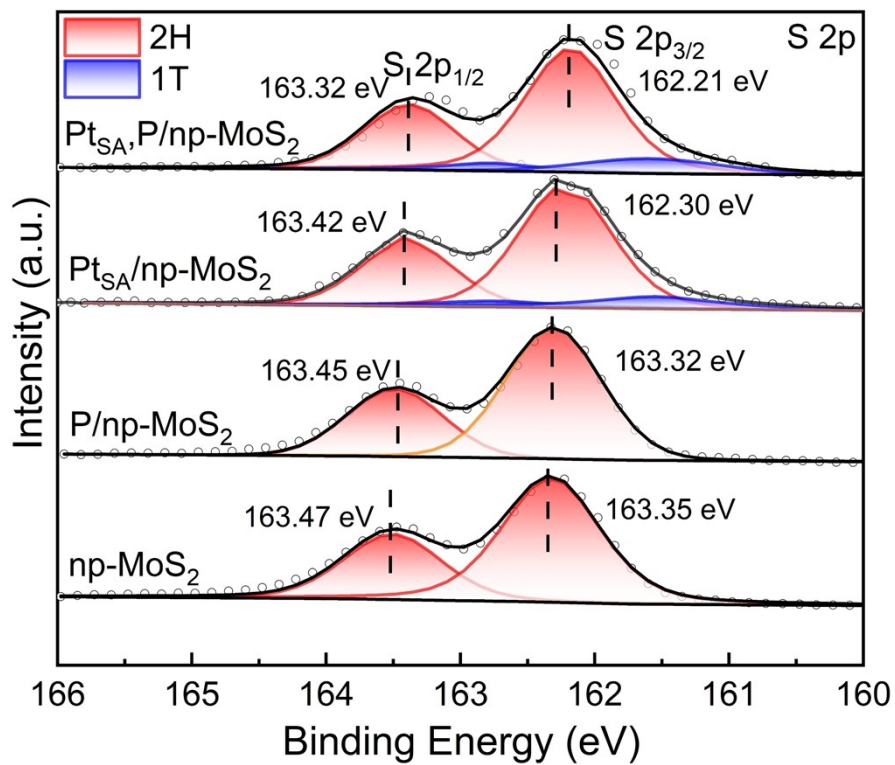
9



1

2 **Figure S4.** SEM characterizations of Pt_{SA}, P/np-MoS₂@NPG. Scale bar: 1 μ m.

3



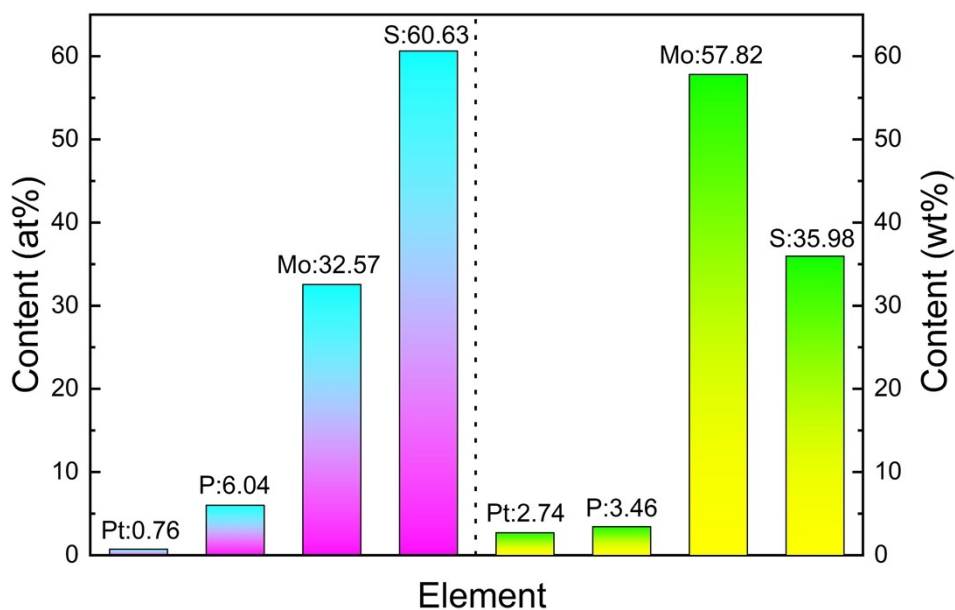
4

5 **Figure S5.** High-resolution XPS spectra of S 2p belong to np-MoS₂, P/np-MoS₂, Pt_{SA}/np-MoS₂, and Pt_{SA},

6 P/np-MoS₂.

7

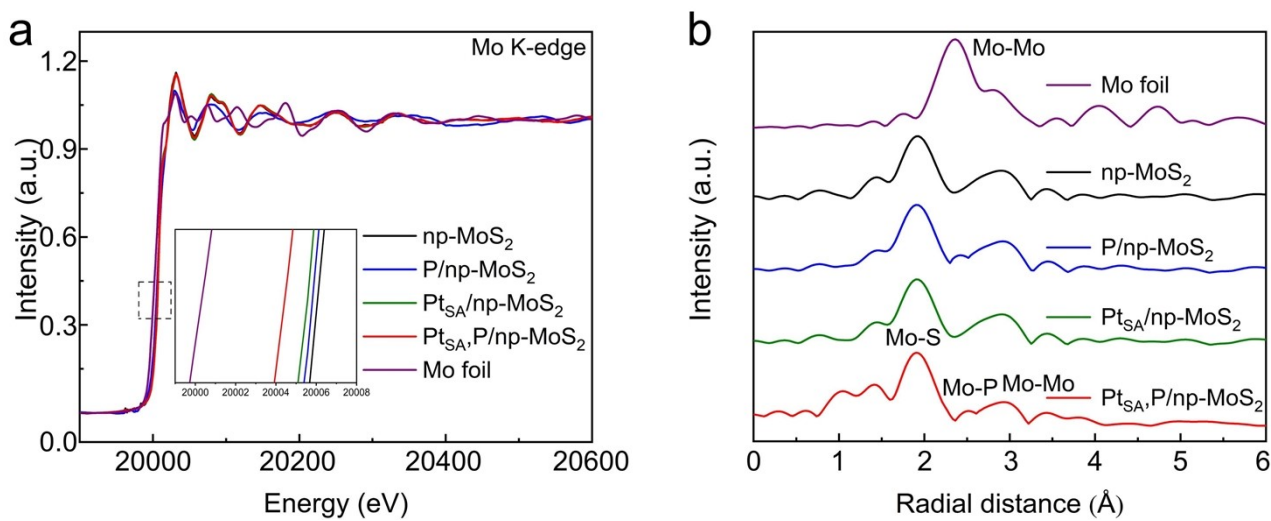
1
2



3

4 **Figure S6.** ICP-OES analysis of Pt_{SA}, P/np-MoS₂. The Pt content is very low.

5



6

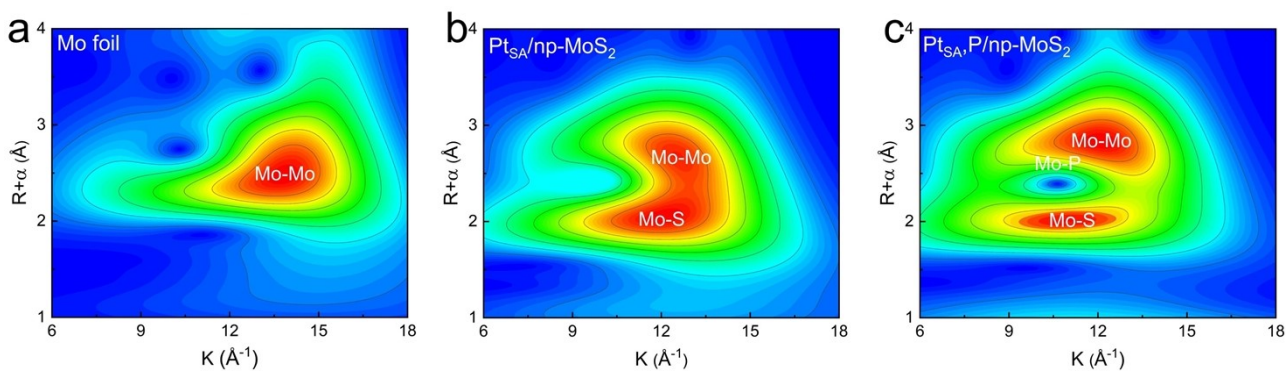
7 **Figure S7.** (a) Mo K-edge XANES spectra of np-MoS₂, P/np-MoS₂, Pt_{SA}/np-MoS₂, Pt_{SA}, P/np-MoS₂, and

8 Mo foil. (b) Corresponding FT-EXAFS spectra from (a).

9

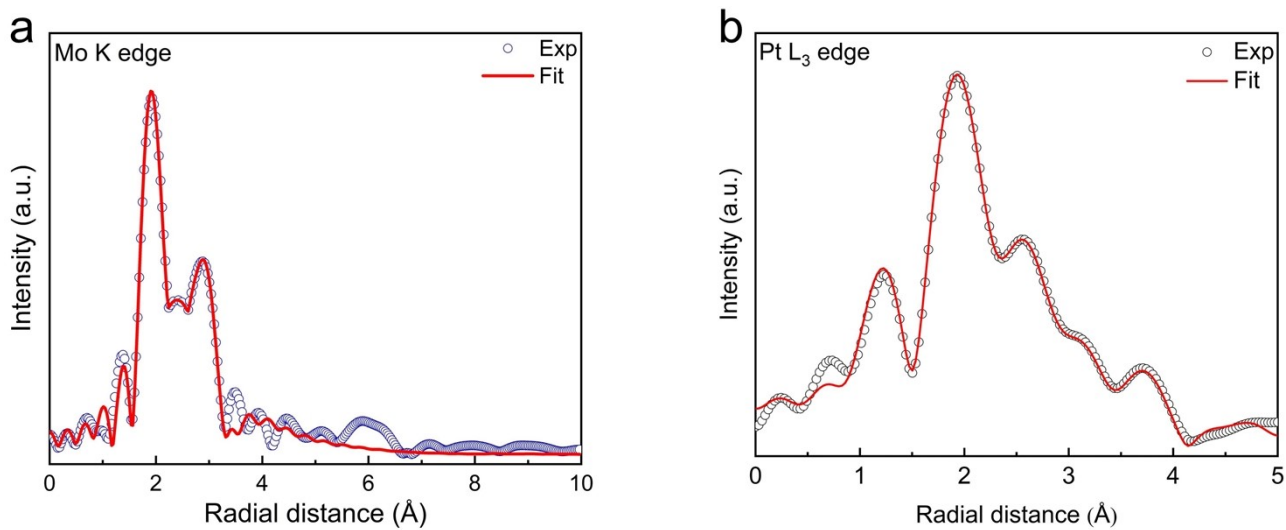
10

11



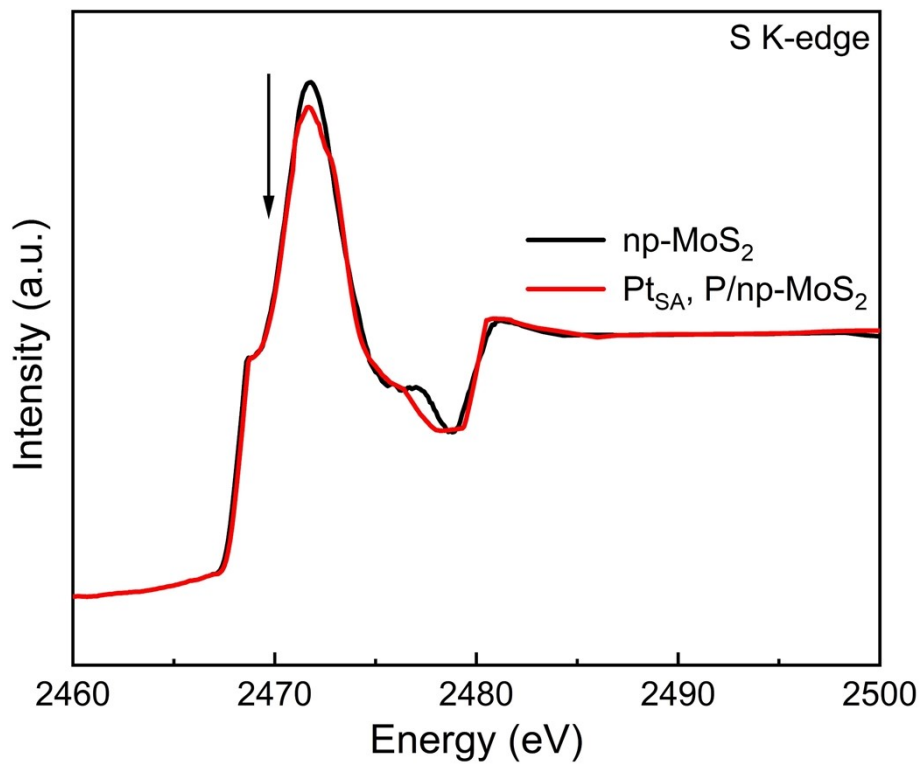
1
2 **Figure S8.** Wavelet transforms of (a) Mo foil, (b) Pt_{SA}/np-MoS₂, and (c) Pt_{SA}, P/np-MoS₂.

3
4
5
6



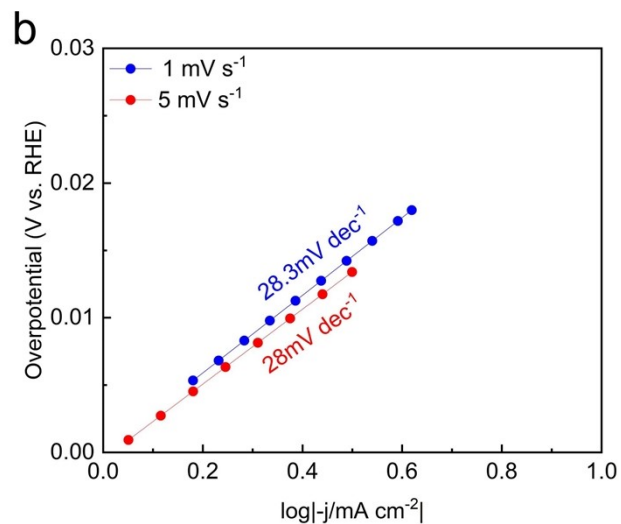
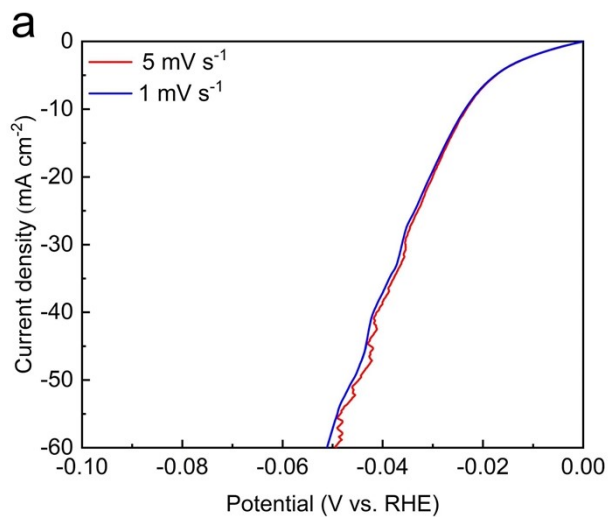
7
8 **Figure S9.** The fitting FT-EXAFS of (a) Mo K-edge and (b) Pt L₃-edge in Pt_{SA}, P/np-MoS₂ with the
9 different fitting paths.

10



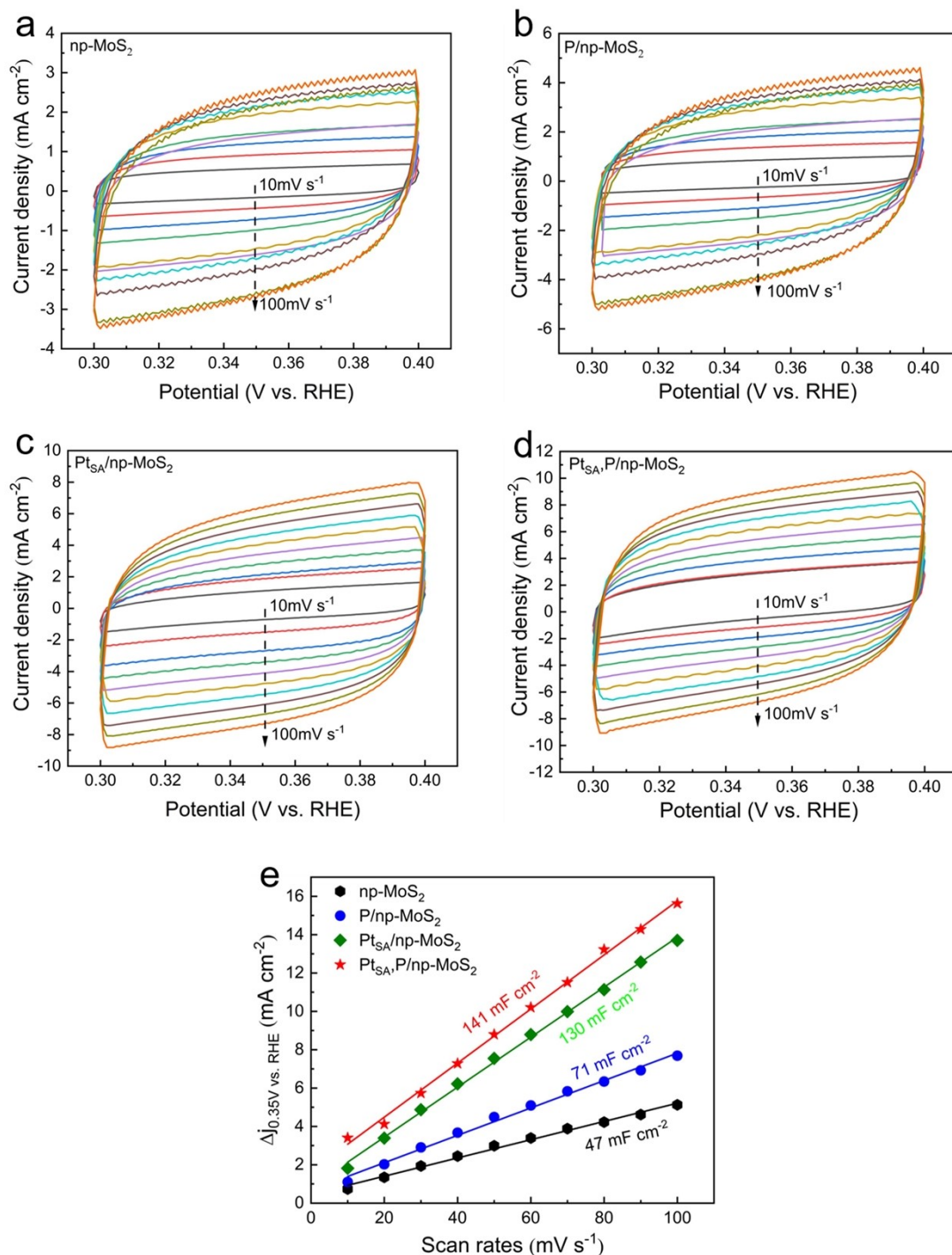
1
2 **Figure S10.** S K-edge XANES spectra of np-MoS₂ and Pt_{SA}, P/np-MoS₂.

3
4
5
6
7
8
9



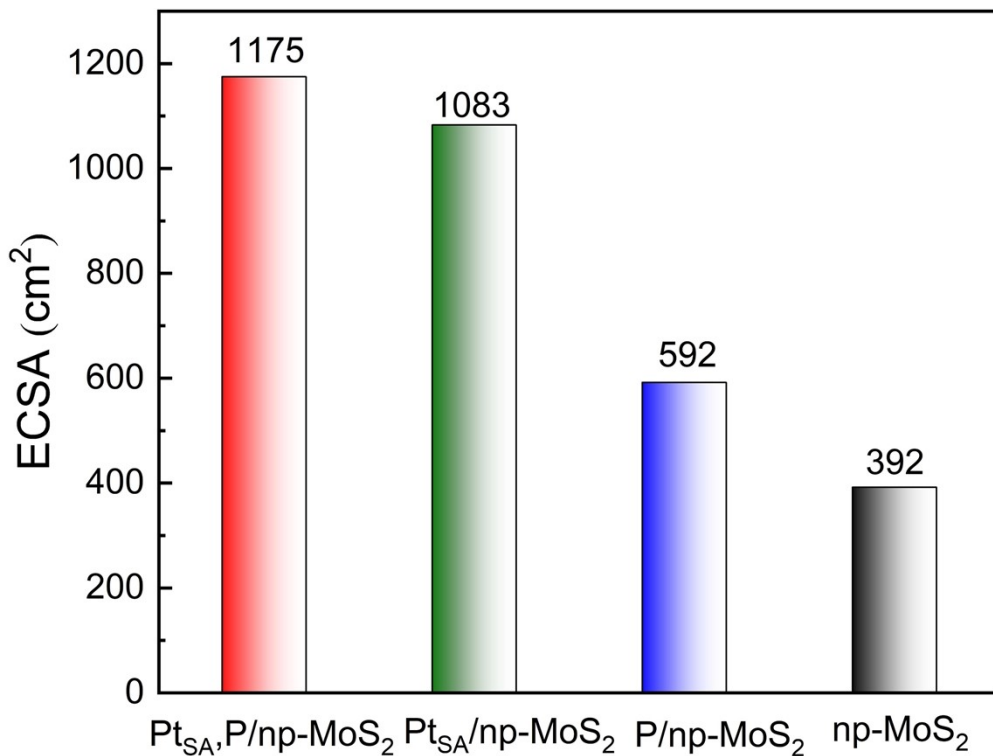
1
 2 **Figure S11.** (a) HER polarization curves of Pt_{SA}, P/np-MoS₂ at different scan rates. (b) Corresponding Tafel
 3 plots derived from (a).

4



1

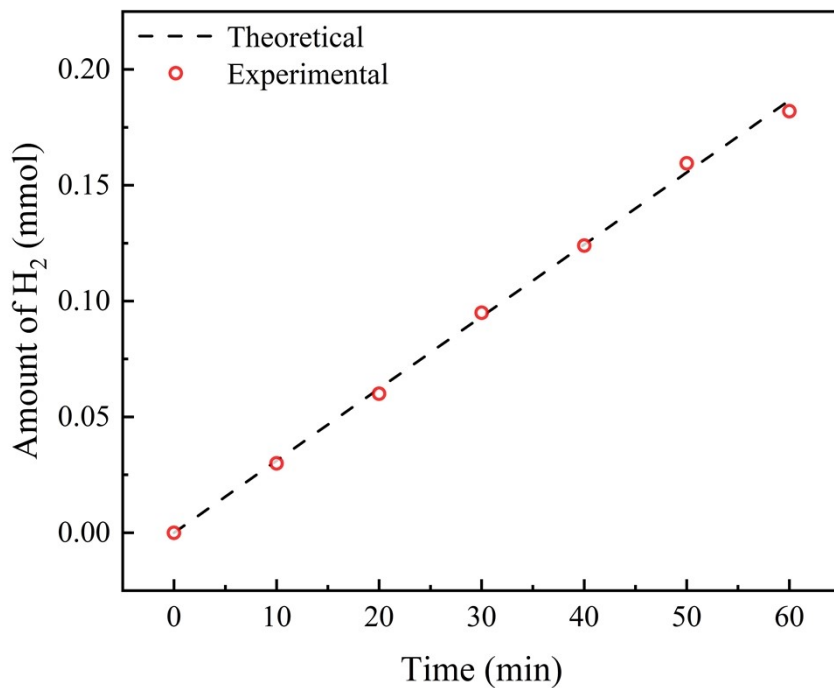
2 **Figure S12.** CV curves at various scan rates (10, 20, 30, 40, 50, 60, 70, 80, 90, and 100 mV s⁻¹) of (a) np-
 3 MoS₂, (b) P/np-MoS₂, (c) Pt_{SA}/np-MoS₂, (d) Pt_{SA}, P/np-MoS₂ in 0.5M H₂SO₄ solution at the potential range
 4 of 0.30 to 0.40 V (vs. RHE). (e) The scaling relationship between Δj (the difference between anodic and
 5 cathodic current densities at 0.35 V) and scan rates for np-MoS₂, P/np-MoS₂, Pt_{SA}/np-MoS₂, and Pt_{SA}, P/np-
 6 MoS₂.



1

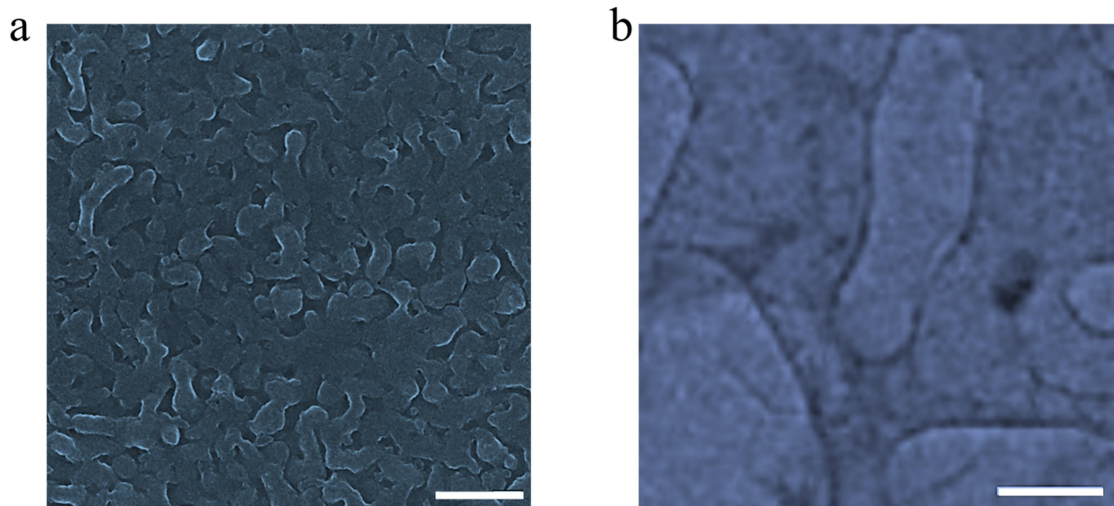
2 **Figure S13.** The real ECSA of np-MoS₂, P/np-MoS₂, Pt_{SA}/np-MoS₂, and Pt_{SA}, P/np-MoS₂. The ECSA
 3 value was calculated based on the equation of $ECSA=C_{dl}/C_s$, where C_s is the specific capacitance. In this
 4 work, the C_s is assumed as 60 $\mu\text{F cm}^{-2}$.

5



6

7 **Figure S14.** Faradaic efficiency of hydrogen evolution of Pt_{SA}, P/np-MoS₂.



1

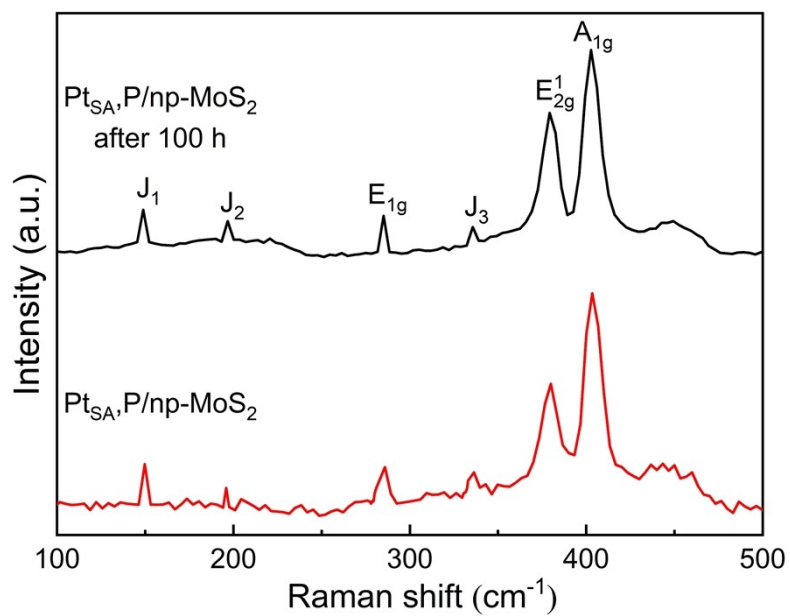
2 **Figure S15.** The (a) SEM image and (b) TEM image of Pt_{SA}, P/np-MoS₂ after HER test for 100 h. Scale

3 bar: (a) 300 nm (b) 200 nm.

4

5

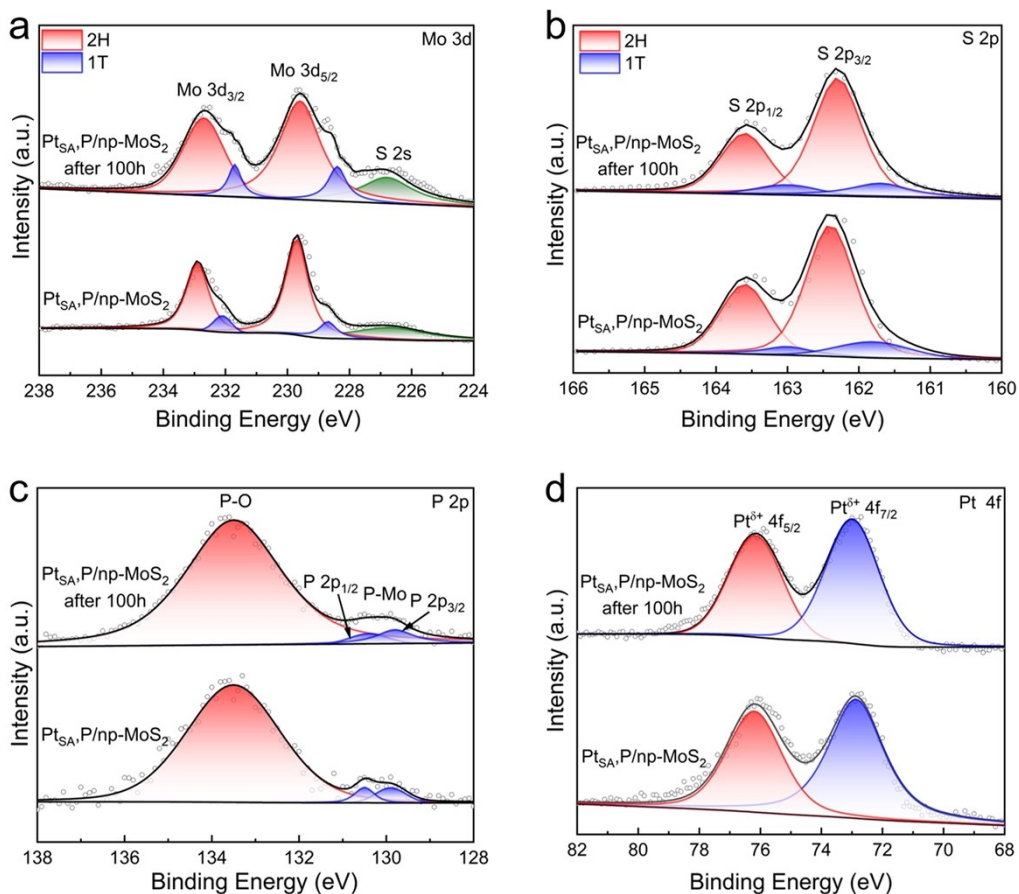
6



7

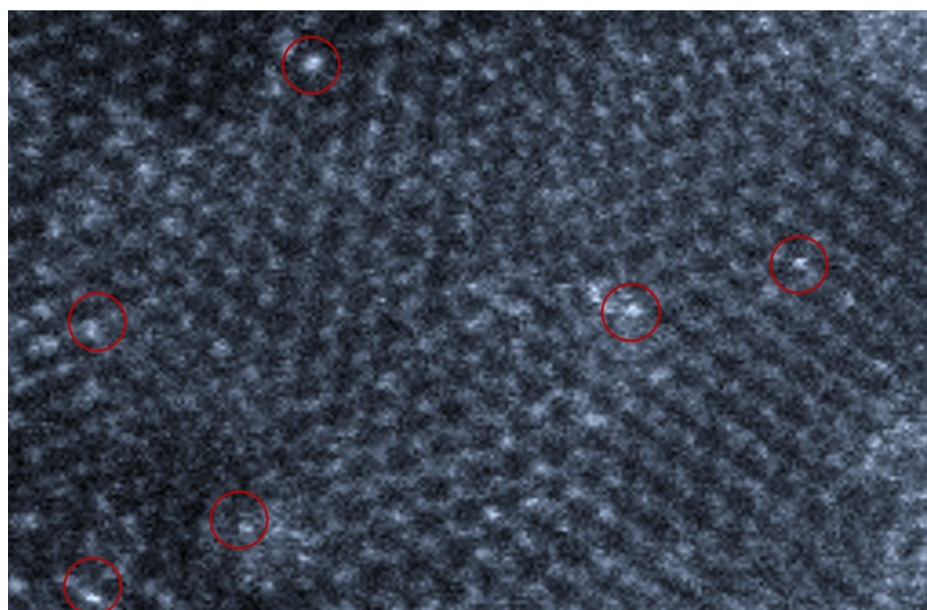
8 **Figure S16.** The Raman spectra of initial Pt_{SA}, P/np-MoS₂ and Pt_{SA}, P/np-MoS₂ after cycling 100 h.

9

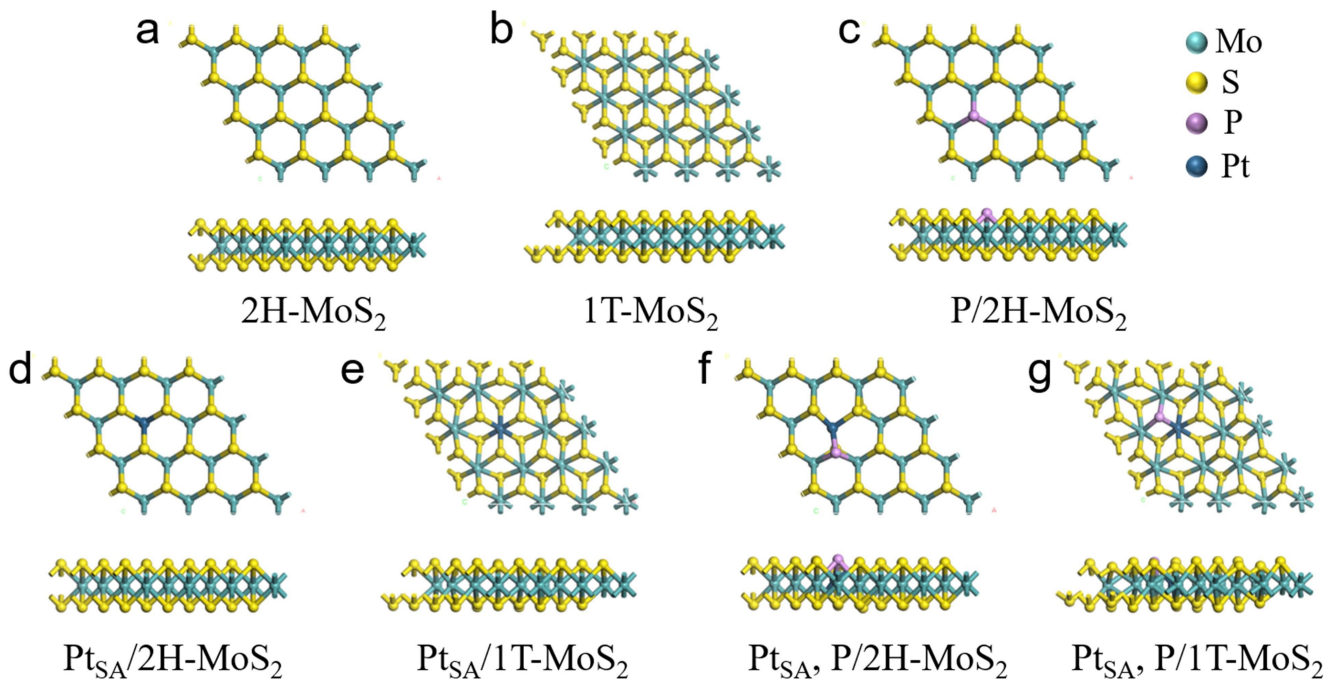


1
 2 **Figure S17.** High-resolution XPS spectra of initial and final (after cycling 100 h) (a) Mo 3d, (b) S 2p, (c)
 3 P 2p, and (d) Pt 4f.

4
 5



6
 7 **Figure S18.** Magnified HAADF-STEM image of Pt_{SA}, P/np-MoS₂ after cycling 100 h, showing the
 8 existence of isolated Pt atoms (red circles). Scale bar: 2 nm



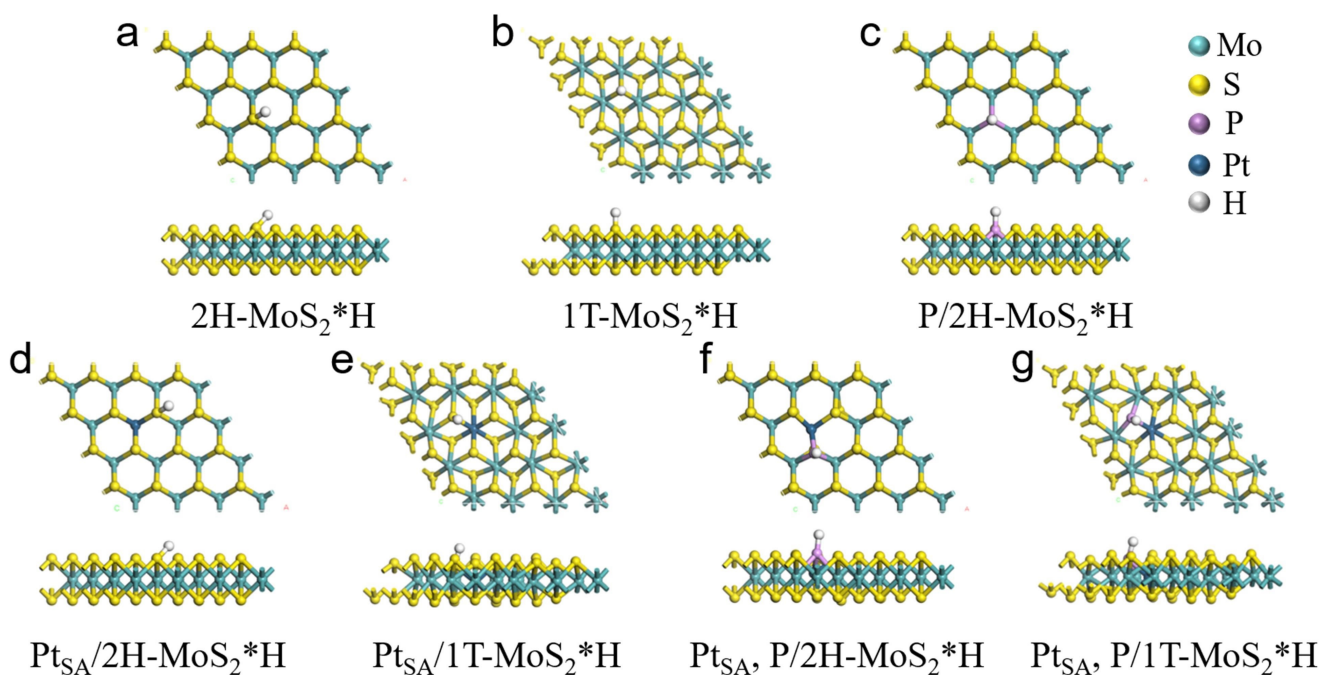
1

2 **Figure S19.** Optimized atomic configurations of top-view and side-view structures of (a) 2H-MoS₂, (b) 1T-
 3 MoS₂, (c) P/2H-MoS₂, (d) Pt_{SA}/2H-MoS₂, (e) Pt_{SA}/1T-MoS₂, (f) Pt_{SA}, P/2H-MoS₂, (g) Pt_{SA}, P/1T-MoS₂.

4

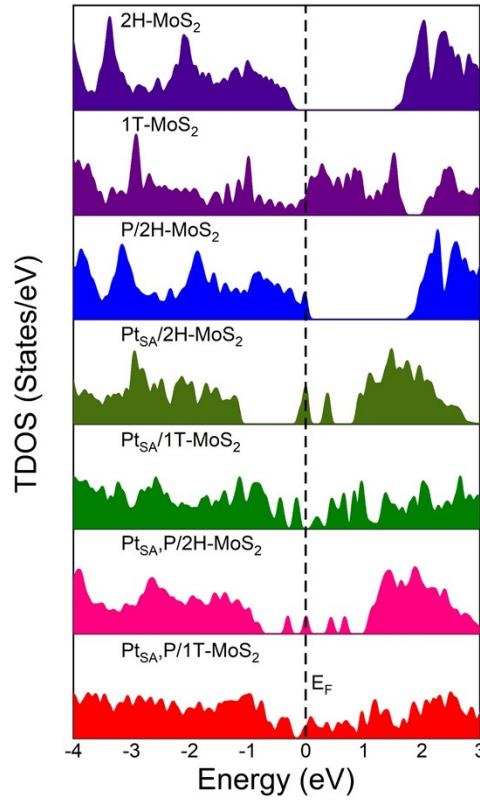
5

6



7

8 **Figure S20.** H* adsorption on (a) 2H-MoS₂, (b) 1T-MoS₂, (c) P/2H-MoS₂, (d) Pt_{SA}/2H-MoS₂, (e) Pt_{SA}/1T-
 9 MoS₂, (f) Pt_{SA}, P/2H-MoS₂, (g) Pt_{SA}, P/1T-MoS₂.



1

2 **Figure S21.** TDOS distribution of 2H-MoS₂, 1T-MoS₂, P/2H-MoS₂, Pt_{SA}/2H-MoS₂, Pt_{SA}/1T-MoS₂, Pt_{SA},
 3 P/2H-MoS₂, Pt_{SA}, P/1T-MoS₂.

4

5 **Table S1.** The atomic ratio and weight ratio data of all elements in np-MoS₂, P/np-MoS₂, Pt_{SA}/np-MoS₂,
 6 and Pt_{SA}, P/np-MoS₂ from XPS result.

Catalysts	np-MoS ₂		P/np-MoS ₂			Pt _{SA} /np-MoS ₂			Pt _{SA} , P/np-MoS ₂			
	Mo	S	P	Mo	S	Pt	Mo	S	Pt	P	Mo	S
Atomic %	34.56	65.44	7.12	33.24	59.64	0.74	34.15	65.11	0.74	6.94	32.07	60.25
Weight %	61.25	48.75	4.14	59.93	35.93	2.62	59.48	37.90	2.69	4.00	57.32	35.99

7

8 **Table S2.** Structural parameters extracted from the EXAFS fitting of Pt_{SA}, P/np-MoS₂.

Catalysts	Scattering path	CN	R (Å)	$\sigma^2(10^{-3} \text{Å}^2)$	ΔE_0 (eV)	R-factor
Pt _{SA} , P/np- MoS ₂	Mo-S	5.49	2.41	3.18	3.82	0.01
	Mo-P	5.23	2.52	3.06	3.15	0.01
	Mo-Mo	6.21	3.17	4.24	1.56	0.01

Pt _{SA} , P/np- MoS ₂	Pt-P/S	3.6	2.09	5.13	4.064	0.0053
---	--------	-----	------	------	-------	--------

1 Note: CN represents the coordination number; R represents the interatomic distance; σ^2 represents the
2 Debye-Waller factor; ΔE_0 represents the edge-energy shift.

3

4 **Table S3.** Comparison of overpotential at 10 mA cm⁻² and Tafel slope of Pt_{SA}, P/np-MoS₂ with recently
5 reported MoS₂-based catalysts in 0.5 M H₂SO₄.

Catalysts	Electrolyte	$\eta@10\text{mA}$ cm ⁻² (mV)	Tafel slope (mV dec ⁻¹)	Reference
Pt _{SA} , P/np-MoS ₂	0.5 M H ₂ SO ₄	30	29	This work
MCM@MoS ₂ -Ni	0.5 M H ₂ SO ₄	53	81	(6) ¹⁴
CoS ₂ @WS ₂ /CC	0.5 M H ₂ SO ₄	97.2	66.0	(7) ¹⁵
Pd, Re-MoS ₂	0.5 M H ₂ SO ₄	46	72	(8) ¹⁶
Cu-Pd-MoS ₂	0.5 M H ₂ SO ₄	93	74	(9) ¹⁷
P, Se-MoS ₂ /CNTs	0.5 M H ₂ SO ₄	110	49	(10) ¹⁸
1% Pd-MoS ₂ /CC	0.5 M H ₂ SO ₄	78	62	(11) ¹⁹
Pt@MoS ₂	0.5 M H ₂ SO ₄	88.43	55.69	(12) ²⁰
MoS ₂ ML	0.5 M H ₂ SO ₄	90	94	(13) ²¹

MoS ₂ /Graphene	0.5 M H ₂ SO ₄	110	67.4	(14) ²²
Ni ₂ P/MoS ₂ /N:RGO	0.5 M H ₂ SO ₄	39.5	39.52	(15) ²³
P-MoS ₂ @HCMF	0.5 M H ₂ SO ₄	86	42.35	(16) ²⁴
MoS ₂ @Pt-3	0.5 M H ₂ SO ₄	70	36	(17) ²⁵
CoFe@NDC@MoS ₂	0.5 M H ₂ SO ₄	64	45	(18) ²⁶

1

2 References

- 3 1. Y. Tan, P. Liu, L. Chen, W. Cong, Y. Ito, J. Han, X. Guo, Z. Tang, T. Fujita, A. Hirata and M. W.
4 Chen, *Adv. Mater.*, 2014, **26**, 8023-8028.
- 5 2. D. Chen, Z. Wei, M. Wang, S. Zhao, P. Liu, A. Pan and Y. Tan, *Nano Lett.*, 2022, **22**, 7020-7027.
- 6 3. Y.-C. Chen, A.-Y. Lu, P. Lu, X. Yang, C.-M. Jiang, M. Mariano, B. Kaehr, O. Lin, A. Taylor, I. D.
7 Sharp, L.-J. Li, S. S. Chou and V. Tung, *Adv. Mater.*, 2017, **29**, 1703863.
- 8 4. D. Voiry, R. Fullon, J. Yang, C. de Carvalho Castro e Silva, R. Kappera, I. Bozkurt, D. Kaplan, M.
9 J. Lagos, P. E. Batson, G. Gupta, Aditya D. Mohite, L. Dong, D. Er, V. B. Shenoy, T. Asefa and
10 M. Chhowalla, *Nat Mater*, 2016, **15**, 1003-1009.
- 11 5. S. Anantharaj, S. Noda, M. Driess and P. W. Menezes, *Acs Energy Lett*, 2021, **6**, 1607-1611.
- 12 6. D. Chen, R. Lu, R. Yu, Y. Dai, H. Zhao, D. Wu, P. Wang, J. Zhu, Z. Pu, L. Chen, J. Yu and S. Mu,
13 *Angew. Chem. Int. Ed.*, 2022, **61**, e202208642.
- 14 7. J. Li, Y. Li, J. Wang, C. Zhang, H. Ma, C. Zhu, D. Fan, Z. Guo, M. Xu, Y. Wang and H. Ma, *Adv.*
15 *Funct. Mater.*, 2022, **32**, 2109439.

- 1 8. G. Kresse and J. Furthmüller, *Phys. Rev. B*, 1996, **54**, 11169.
- 2 9. J. P. Perdew, K. Burke and M. Ernzerhof, *Phys. Rev. Lett.*, 1996, **77**, 3865.
- 3 10. P. E. Blöchl, *Phys. Rev. B*, 1994, **50**, 17953-17979.
- 4 11. G. Kresse and D. Joubert, *Phys. Rev. B*, 1999, **59**, 1758.
- 5 12. S. Grimme, J. Antony, S. Ehrlich and H. Krieg, *J. Chem. Phys.*, 2010, **132**, 154104.
- 6 13. E. Santos, P. Quaino and W. Schmickler, *Phys. Chem. Chem. Phys.*, 2012, **14**, 11224-11233.
- 7 14. H. B. Zhang, L. Yu, T. Chen, W. Zhou and X. W. Lou, *Adv. Funct. Mater.*, 2018, **28**, 1807086.
- 8 15. X. F. Zhou, X. L. Yang, H. N. Li, M. N. Hedhili, K. W. Huang, L. J. Li and W. J. Zhang, *J. Mater.*
9 *Chem. A*, 2017, **5**, 15552-15558.
- 10 16. Z. Y. Luo, J. J. Li, Y. L. Li, D. J. Wu, L. Zhang, X. Z. Ren, C. X. He, Q. L. Zhang, M. Gu and X.
11 L. Sun, *Adv. Energy Mater.*, 2022, **12**, 2103823.
- 12 17. D. C. Han, Z. Y. Luo, Y. Li, N. X. Gao, J. J. Ge, C. P. Liu and W. Xing, *Appl. Surf. Sci.*, 2020,
13 **529**, 147117.
- 14 18. T. Zhu, J. B. Ding, Q. Shao, Y. Qian and X. Q. Huang, *Chemcatchem*, 2019, **11**, 689-692.
- 15 19. Z. Y. Luo, Y. X. Ouyang, H. Zhang, M. L. Xiao, J. J. Ge, Z. Jiang, J. L. Wang, D. M. Tang, X. Z.
16 Cao, C. P. Liu and W. Xing, *Nat. Commun.*, 2018, **9**, 2120.
- 17 20. Y. Li, Q. F. Gu, B. Johannessen, Z. Zheng, C. Li, Y. T. Luo, Z. Y. Zhang, Q. Zhang, H. I. Fan, W.
18 B. Luo, B. L. Liu, S. X. Dou and H. K. Liu, *Nano Energy*, 2021, **84**, 105898.
- 19 21. J. Qu, Y. Li, F. Li, T. M. Li, X. Y. Wang, Y. Yin, L. B. Ma, O. G. Schmidt and F. Zhu, *Acs Nano*,
20 2022, **16**, 2921-2927.
- 21 22. L. B. Ma, Y. Hu, G. Y. Zhu, R. P. Chen, T. Chen, H. L. Lu, Y. R. Wang, J. Liang, H. X. Liu, C. Z.
22 Yan, Z. X. Tie, Z. Jin and J. Liu, *Chem. Mater.*, 2016, **28**, 5733-5742.

- 1 23. M. Kim, M. A. R. Anjum, M. Lee, B. J. Lee and J. S. Lee, *Adv. Funct. Mater.*, 2019, **29**, 1809151.
- 2 24. J. Xiong, J. Li, J. W. Shi, X. L. Zhang, W. W. Cai, Z. H. Yang and H. S. Cheng, *Appl Catal B-*
3 *Environ*, 2019, **243**, 614-620.
- 4 25. X. Y. Xu, X. F. Dong, Z. J. Bao, R. Wang, J. G. Hu and H. B. Zeng, *J. Mater. Chem. A*, 2017, **5**,
5 22654-22661.
- 6 26. S. Ali Shah, L. Xu, R. Sayyar, T. Bian, Z. Liu, A. Yuan, X. Shen, I. Khan, A. Ali Tahir and H.
7 Ullah, *Chem. Eng. J.*, 2022, **428**, 132126.

8